

Finite element analyses of the stability of a soil block reinforced by shear pins

Rithy Ouch^{1a}, Boonchai Ukritchon^{*1},
Thirapong Pipatpongsa^{2b} and Mohammad Hossein Khosravi^{3c}

¹ Geotechnical Research Unit, Department of Civil Engineering, Chulalongkorn University, Bangkok, Thailand

² Department of Urban Management, Kyoto University,
Katsura Campus, Nishikyo-ku, Kyoto, 615-8540, Japan

³ School of Mining Engineering, College of Engineering, University of Tehran, Tehran, Iran

(Received May 16, 2016, Revised October 01, 2016, Accepted February 02, 2017)

Abstract. The assessment of slope stability is an essential task in geotechnical engineering. In this paper, a three-dimensional (3D) finite element analysis (FEA) was employed to investigate the performance of different shear pin arrangements to increase the stability of a soil block resting on an inclined plane with a low-interface friction plane. In the numerical models, the soil block was modeled by volume elements with linear elastic perfectly plastic material in a drained condition, while the shear pins were modeled by volume elements with linear elastic material. Interface elements were used along the bedding plane (bedding interface element) and around the shear pins (shear pin interface element) to simulate the soil-structure interaction. Bedding interface elements were used to capture the shear sliding of the soil on the low-interface friction plane while shear pin interface elements were used to model the shear bonding of the soil around the pins. A failure analysis was performed by means of the gravity loading method. The results of the 3D FEA with the numerical models were compared to those with the physical models for all cases. The effects of the number of shear pins, the shear pin locations, the different shear pin arrangements, the thickness and the width of the soil block and the associated failure mechanisms were discussed.

Keywords: slope stability; shear pin; numerical model; interface element

1. Introduction

Pile group or pile raft foundations have been employed in practice to support large structures such as high-rise buildings and bridges, etc. Numerous works have been carried out to study the behaviors of pile group or pile raft foundations subjected to vertical or lateral loads (e.g., Madhav *et al.* 2009, Nakanishi and Takewaki 2013, Wu *et al.* 2013, Fatahi *et al.* 2014, Qian *et al.* 2014).

In addition to piles being used in pile group or pile raft foundations to support large structures, the installation of pile rows for slope stabilization is considered an important technique. It has been widely adopted by many researchers in the past (e.g., Ito and Matsui 1975, Ito *et al.* 1982, Poulos

*Corresponding author, Sc.D., Associate Professor, E-mail: boonchai.uk@gmail.com

^a Ph.D. Student, E-mail: rithyouch23@gmail.com

^b D.Eng., Associate Professor, E-mail: pipatpongsa.thirapong.4s@kyoto-u.ac.jp

^c Ph.D., Assistant Professor, E-mail: mh.khosravi@ut.ac.ir

1995, Ausilio *et al.* 2001, Keawsawasvong and Ukritchon 2017). Ito and Matsui (1975) developed an equation to predict the lateral force acting on slope-stabilizing piles. Subsequently, Ito *et al.* (1982) extended that method and proposed the mobilization factor of the lateral force for designing slopes with multiple rows of piles. Poulos (1995) described a process for the design of pile rows for reinforcing slopes by the computer program ERCAP, in which the stress distribution along the installed piles was predicted by the equation of Ito and Matsui (1975). Ausilio *et al.* (2001) presented an analytical expression for predicting the lateral force for increasing the safety factor of slopes reinforced with piles based on the kinematic approach of the limit analysis. They concluded that the best location for piles within a slope is close to the toe of the slope, where the lateral force acting on the piles is the minimum. The most effective pile location was found to be from the toe to the middle of the slope. Wei and Cheng (2009) studied the most suitable location for piles in slope stabilization by means of the two-dimensional finite difference method (FLAC 2D). Their results revealed that the location of piles affects the failure mechanism of the slope; and thus, the piles should be installed in the middle part of the slope to obtain the maximum safety factor. Li *et al.* (2011) used the two-dimensional finite difference method (FLAC 2D) to study a slope reinforced by one row of piles and obtained results similar to those of Wei and Cheng (2009). Kanagasabai *et al.* (2011) employed FLAC 3D to investigate the behavior of slope stabilization by piles, whereby the effects of the variation in strength between the slipping plane and the stable slope layer were considered, and associated failure mechanisms of the soil around the piles were proposed.

Kourkoulis *et al.* (2011, 2012) used the hybrid method to analyze and design a slope stabilized by single piles and pile groups, whereby the pile spacing, the thickness of the stable soil mass, the depth of the pile embedment, the pile diameter and the pile group configuration were investigated. Haigh and Gopal Madabhushi (2011) performed geotechnical centrifuge tests to investigate the pile-soil interaction in liquefiable slopes, in which the pore pressure and the state of stress in both the upslope and the downslope of the pile were studied. Galli and di Prisco (2012) implemented a displacement-based design procedure or coupled analysis for slope stabilization with a single pile. They concluded that the pile-soil interaction force could be predicted based on the displacement-based procedure and vice versa, while a monitoring system was required for the optimum design of a structure. Zhou *et al.* (2014) employed two methods (limit equilibrium method and finite element analysis) to predict the lateral force acting on piles from an unstable slope by considering the effects of the pore water pressure and the strength of the slip zone. Ho (2014) employed a three-dimensional finite element analysis (ABAQUS) to investigate a soil slope that consisted of a weak plane layer reinforced by pile rows. Liang *et al.* (2014) developed a computer program (UASLOPE) to analyze and design a row of drilled shafts to stabilize a slope. Li and Liang (2014) extended their methods to analyze and design multiple rows of drilled shafts to stabilize a slope, where the optimization principles for this problem were discussed. Zhang *et al.* (2015) employed a linear regression analysis to study the failure characteristics of an embankment slope, a sheet-pile wall and the factors influencing the instability of the slope.

Stabilizing drilled shafts or piles are commonly employed as an effective means for a slope or landslide stabilization and include steel driven piles, bored piles, micro piles, soldier piles, stone columns, or shear pins (Pradel *et al.* 2010). Shear pins are made of reinforcement bars or larger steels, concrete or post sections that may be grouted at in-situ. Thus, shear pin is one option of stabilizing drilled shafts to mitigate unstable slopes due to its cost effectiveness and simple construction process. Generally, it is designed to act mainly as a shear member and to be installed perpendicularly to a bedding or potential slip plane. The shear pin provides an additional shear

resistance from an installed steel bar and concrete and frictional interface between soil and concrete surface. In addition to resist a shear force, the shear pin must also withstand a bending moment that arises from a lateral soil pressure of slope. Analysis and design of shear pin for slope stabilization can be performed using a general framework of slope stabilizing drilled shafts such as an approach proposed by Kourkoulis *et al.* (2011, 2012).

As mentioned earlier, studies on the use of piles to stabilize slopes have drawn much attention over the last several years. This paper employs the three-dimensional finite element analysis to investigate the performance of different shear pin arrangements on the increase in stability of a soil block resting on a low-interface friction plane, as shown in Fig. 1. The stability of this problem is attributed to the strength of the soil block and the interface friction plane together with the influence of the shear pins installed inside the soil block. The load-transfer mechanism of the physical models is similar to that of the actual site of an open-pit mine (Khosravi 2012, Pipatpongsa *et al.* 2013). Two types of rock masses (shale and lignite) appear mostly in Area 4.1 of the Mae Moh lignite mine and rest on a bedding plane infilled by clay seams with low interface strength. When the lignite at the toe of the slope is excavated at its full width, a large displacement of the rock mass occurs in the slope part. In order to reduce the displacement and to ensure a

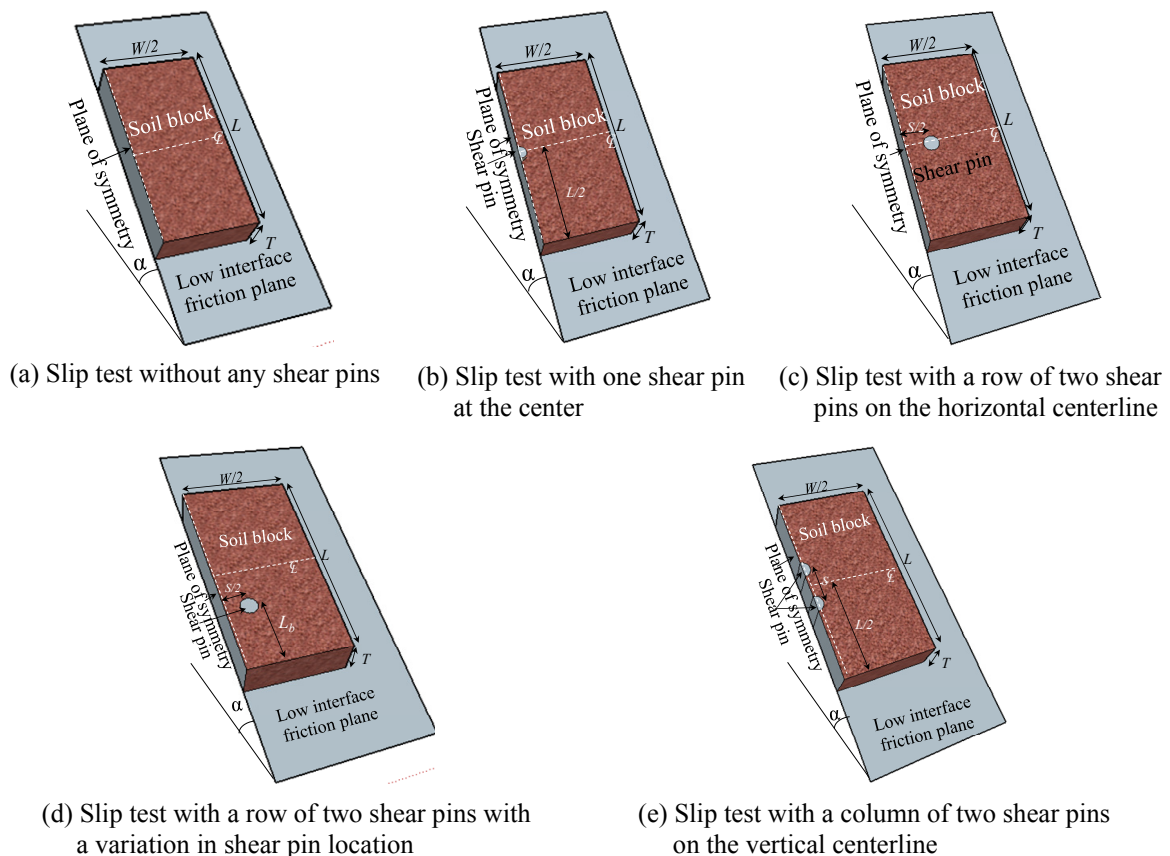


Fig. 1 Problem definition of slip tests of a soil block resting on a low-interface friction plane, with and without shear pins, shown in a half-section along the plane of symmetry

higher level of safety, the Electricity Generating Authority of Thailand (EGAT) decided to install

piles, known as shear pins, with a diameter of 150 mm. The pins were made of steel cable, with a diameter of 50 mm, and were surrounded by mortar. Since the slope stabilization of an undercut slope is comparatively uncommon in surface mining, fundamental knowledge of undercut slope reinforcement is required to further develop the undercut slope design that has been reported in Pipatpongsa *et al.* (2013). As slip resistance tests using a soil block were the primary model tests conducted in past studies for the no-arching case, the previous tests were modified by adding shear pins. Thus, the models studied here will provide a better understanding of the effect of the performance of different shear pin arrangements on the behavior and the failure mechanism, which will be compared with the arching case in subsequent works.

The experiments consisted of slip tests, with and without side supports, and undercut slopes, resting on a low-interface plane. They were studied intensively by Khosravi *et al.* (2011, 2012) and Khosravi (2012). The results of the slip tests showed that the slope failure was due to the shear sliding on the low-interface friction plane. This failure mechanism also occurred together with shear sliding on the side supports for the slip tests with side supports. However, two types of failure were observed for the physical models of the undercut slopes, namely: (1) an arch-shaped failure for mildly undercut slopes; and (2) total failure with upheaval buckling on the pillars for steeply undercut slopes. However, the effects of shear pins on the stability of those tests have not been investigated. Recently, Ouch *et al.* (2016) employed 3D FEA to study the stability and failure mechanism of soil blocks (with and without supports) resting on low interface friction plane.

Previous works on soil slopes stabilized by piles or on soil slopes with a low-interface friction plane are available in the literature. However, not many researches have employed a three-dimensional finite element analysis to investigate soil slopes resting on a low-interface friction plane reinforced with small piles, such as shear pins. Thus, the aim of this research is to investigate the effect of the performance of different shear pin arrangements on the stability of a soil block resting on a low-interface friction plane by means of a three-dimensional finite element analysis, as schematically summarized in Fig. 1. The results of the analysis and the experiments are compared. Conclusions will be drawn about the effects of the number of shear pins, the shear pin locations, the different shear pin arrangements and the thickness and the width of the soil slope, which increase the stability of a soil block with a low-interface friction plane.

2. Overview of experimental tests

Physical models of slip tests with and without shear pins are shown in Fig. 2. The soil block has length L , width W , thickness T and angle α measured from the horizontal plane resting on a relatively low-interface friction plane. The location of the pins, L_b , is measured from the bottom edge of the soil block. In the experimental models, a wooden plate, 2.5 cm in thickness, 40 cm in width and 60 cm in length, was used as the basal support. The plate was covered by a Teflon film to simulate the low-interface friction plane.

Steel screw bolts M4, 4 mm in diameter and 70 mm in length, were selected as the shear pins to stabilize the soil block in all tests, where they can represent the case of rigid piles in the field. The bolt length of 7 cm was chosen to match with tests with model thickness, $T = 1\text{--}5$ cm. The pins were screwed 2 cm deep into the wooden plate perpendicularly on the slope model and the sand was later filled and compacted. Humid silica sand, with a controlled bulk density and water content, was compacted on the Teflon film inside a wooden frame. The entire soil block was built by carefully compacting soil layers while controlling the soil weight. In addition, a small wooden plate, 3 cm in width, 10 cm in length and 2 cm in thickness, was used to effectively compact the

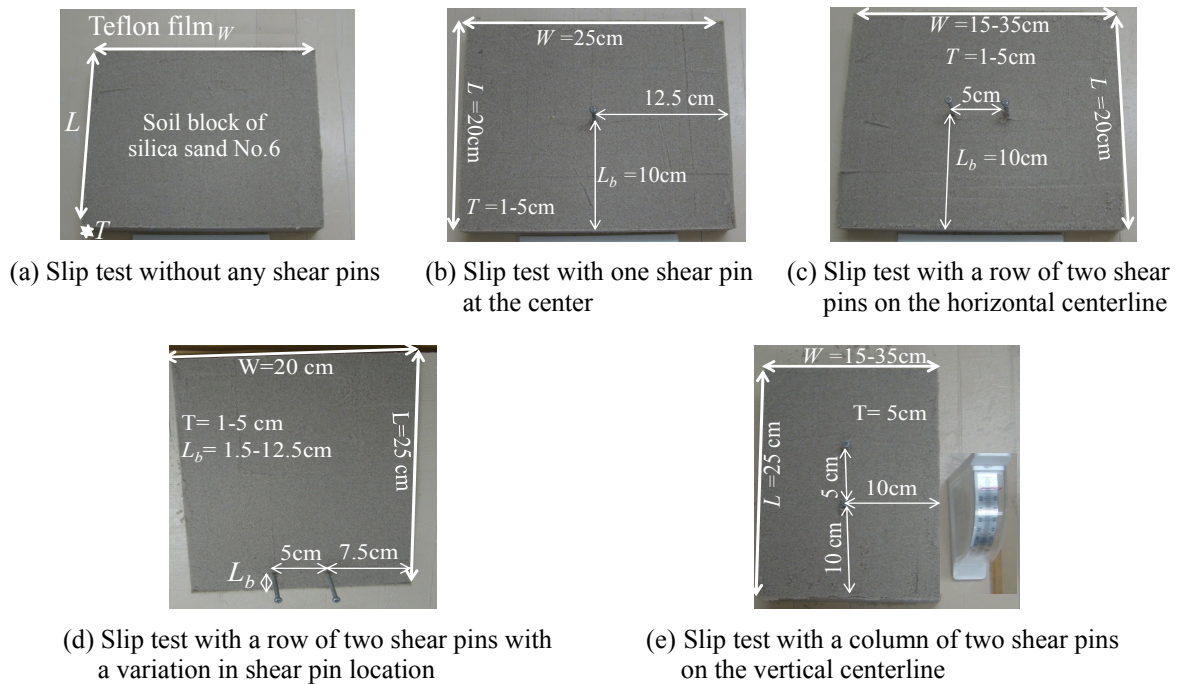


Fig. 2 Geometry of slip tests with and without shear pins

sand close to the shear pins. After completing the compaction, the frame was removed and the wooden plate was gradually tilted until the soil block started slipping. The failure slope angle was then recorded. The slip test without any shear pins was conducted in a similar way to the tests with shear pins.

This study employed humid silica sand and preparation of soil block that were the same as previous studies by Khosravi (2012). Fig. 3 shows the result of direct shear test of humid silica sand, where its apparent cohesion (c) and the friction angle (ϕ) are: $c = 8 \text{ kN/m}^2$ and $\phi = 41.5^\circ$. Non-zero cohesion of humid silica sand was due to an effect of negative capillary pressure in an unsaturated soil with a water content of 10%, resulting in an “apparent” cohesion. The grain size distribution of humid silica sand is shown in Fig. 4, where its average grain size is 0.32 mm with a soil classification of SP. The interface apparent cohesion (c_i) and friction angle (ϕ_i) of the bedding plane are: $c_i = 0.06 \text{ kN/m}^2$, $\phi_i = 22^\circ$, as shown in Fig. 5, where they were obtained from direct shear tests by putting humid silica sand on top of the Teflon film.

The effect of the shear pin arrangement was studied by a couple of shear pins installed with a fixed spacing, but with a different alignment along the length and the width of the soil block. The spacing between the shear pins was kept constant at 5 cm, namely, 12.5 times the shear pin diameter. In total, five parametric studies of slip tests for the soil block were carried out: 1) slip test without any shear pins (Figs. 1(a)-2(a)); 2) slip test with one shear pin at the center (Figs. 1(b)-2(b)); 3) slip test with a row of two shear pins on the horizontal centerline (Figs. 1(c)-2(c)); 4) slip test with a row of two shear pins with a variation in shear pin locations (Figs. 1(d)-2(d)); and 5) slip test with a column of two shear pins on the vertical centerline (Figs. 1(e)-2(e)). Herein, the terms “column” and “row” represent the lengthwise and the crosswise alignments of the shear pins, respectively.

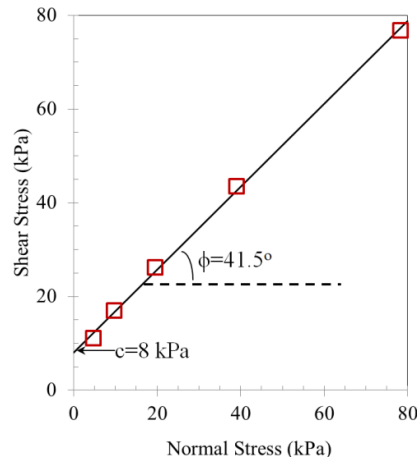


Fig. 3 Direct shear test results of humid silica sand

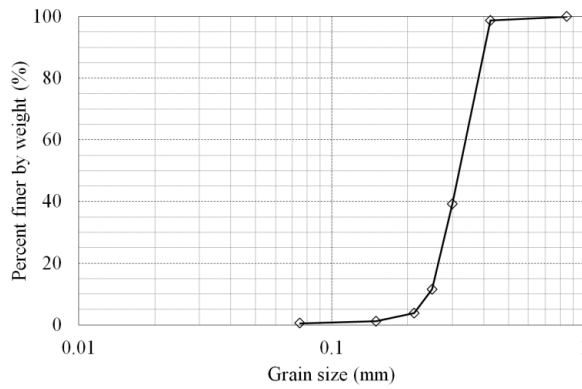


Fig. 4 Grain size distribution of humid silica sand

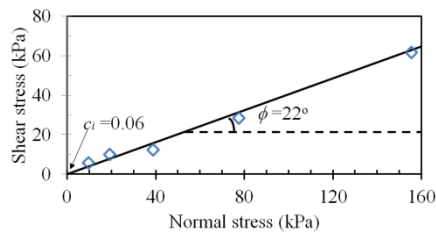


Fig. 5 Direct shear test results of interface properties between humid silica sand and Teflon film

3. Three-dimensional finite element analysis

In this study, Plaxis 3D version 2013 (Brinkgreve 2012), a three-dimensional (3D) finite element program, is employed to analyze the stability of a soil block with shear pins resting on a low-interface friction plane. The 3D finite element models correspond to the slip test of physical models with and without shear pins, as schematically shown in Fig. 6.

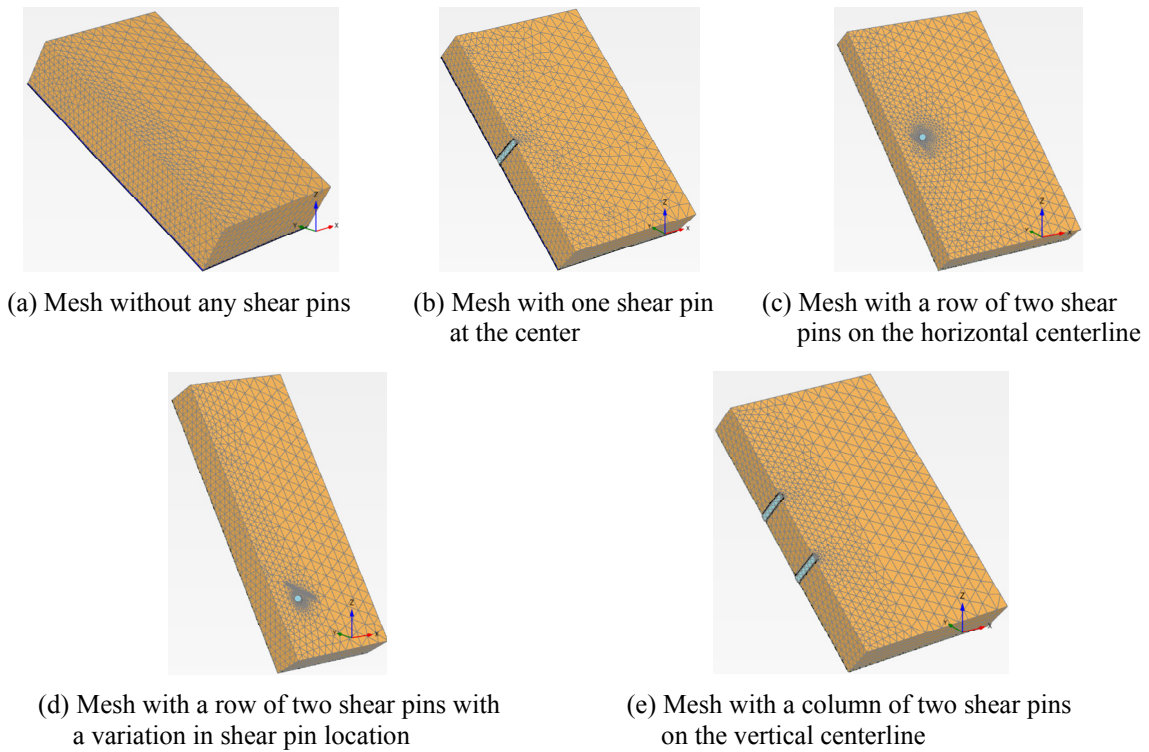


Fig. 6 Mesh layouts of a half-section of soil block used in slip tests with and without shear pins

Due to the symmetry in all the experiments, only half of the numerical model is used in the finite element simulation in order to shorten the computational time. The soil block and the shear pin are modeled by volume elements while the bottom plane is modelled as the plate element. Interface elements are employed at the low-interface friction plane and around the shear pin. The bottom boundaries of the plate elements and the shear pin volume elements are fixed in all directions. The symmetrical plane of the soil block is fixed only in the x -axis ($u_x = 0$), while the other directions are free ($u_y = u_z = \text{free}$). Sufficiently fine mesh element distributions are set up for all the models to obtain accurate solutions, as shown in Fig. 6. 10-node tetrahedral elements are used for the volume elements, while 6-node elements are used for the plate elements. The 6-node interface elements are used to simulate the soil-structure interaction behavior, where they are placed between the bottom plate and the soil block as well as around the shear pins and the surrounding soil. The same modeling techniques are also employed in the case without any shear pins.

The geometry and the material properties inputted into the numerical models are the same as those in the physical models, as explained in the previous section. The input parameters of material properties of the soil block and the shear pins are summarized in Tables 1 and 2 while those of the interface elements between the shear pins and the sand, and the interface elements between the Teflon film and the sand at the bedding plane are summarized in Tables 3 and 4. Both soil volumes and interface elements are assigned as Mohr-Coulomb material with the associated flow rule in the drained condition. The dilatancy angle of the soil is equal to the internal friction angle because of the associated flow rule. Khosravi (2012) suggested that the apparent soil cohesion of 8 kPa

Table 1 Input parameters of the soil block for the finite element analysis

Mohr-Coulomb	Value
Young's modulus, E	4000 kN/m ²
Poisson's ratio, ν	0.3
Apparent cohesion, c	0.358 kN/m ²
Friction angle, ϕ	41.5°
Dilatancy angle, ψ	41.5°

Table 2 Input parameters of the shear pin for the finite element analysis

Linear elastic	Value
Young's modulus, E	200000 MN/m ²
Unit Weight, γ	78.50 kN/m ³
Poisson's ratio, ν	0.3

Table 3 Input parameters of the interface element between the shear pin and the soil

Soil-pin interface parameters	Value
Interface friction angle	41.5°
Interface apparent adhesion	0.358 kN/m ²

Note: The properties of the interface shear pin are the same as those of the adjacent soil for the fully rough condition

Table 4 Input parameters of the interface element between the Teflon film and the soil at the bedding plate

Soil-Teflon film interface	Value
Interface friction angle	22°
Interface apparent adhesion	0.06 kN/m ²

obtained from direct shear tests on humid silica sand was refined to 0.358 kPa to match the measured data from unconfined compression tests assuming the same friction angle of 41.5°. Thus, this value of 0.358 kPa is used as the input apparent cohesion of humid silica sand for finite element analyses. Poisson's ratio of the soil block is 0.3 following typical drained material. A linear elastic material is used for the plate element of the bottom plane, where its Young's modulus is set at a relatively high value in order to simulate the rigid support.

Since the observed failures of all physical models happened due to the shear sliding along the low-interface friction plane and the failure of soil block itself while there was no failure of shear pin, the shear pins in finite element analyses are modelled as an elastic material, where their mechanical properties correspond to these of steel. Considering the average sand grain size of 3.2 mm and the size of steel crew bolt, it is assumed that a possible interaction between the lateral surface of the steel screw bolt and the sand grain should correspond to a fully rough surface of interface. For this condition, the "apparent" cohesion and friction angle at the soil-shear pin interface is the same as these of the sand, where they were used as input properties in finite

element analyses. To check this assumption, a fully smooth surface was also modelled for some cases, as explained in the section of results.

In this study, a failure analysis is performed by means of the gravity loading method (Brinkgreve *et al.* 2013). The weight multiplier ($\Sigma Mstage$) is increased automatically by Plaxis3D in such a way that the applied unit weight is equal to the product of the input unit weight (γ_{input}) and the applied $\Sigma Mstage$ value. The simulation of the weight increment is performed by the automatic load control of the iterative finite element procedure. The state of failure in the finite element analysis is defined by the convergence of the $\Sigma Mstage$ to a certain value, or the $\Sigma Mstage$ value cannot be increased further during two successive calculation steps, giving rise to the failure value of $\Sigma Mstage_f$. Accordingly, the failure unit weight (γ_f) is obtained by the product of $\Sigma Mstage_f$ and the input unit weight (γ_{input}), namely

$$\gamma_f = \Sigma Mstage_f \times \gamma_{input} \quad (1)$$

It is worth noting that the state of stress of the soil volume in the gravity loading method starts from zero and is increased by an iterative elasto-plastic finite element procedure until failure. This is contrast to that in the experimental test, where it is not zero at the initial condition. The effect of initial state of stress in the soil volume is not considered in this study since stability and failure mechanism are the major concerns in finite element simulation. Initial state of stress and applied stress path have a profound influence on an observed deformation of a problem prior to failure, but not at the limit state. This is justified by the framework of limit analysis, where a solution at the limit state is only affected by strength properties of material, not by its initial state of stress provided that the geometry is essentially unaltered (see Chen 1975). Thus, the stability and failure mechanism of this problem only depends on the strength properties of soil block, interface, and a unit weight of soil that is the driving force of the problem. Consequently, at the limit state, there should be no significant error associated with neglecting initial state of stress in the soil volume in the finite element method with the gravity loading method. In addition, the gravity loading method was proposed by Griffiths and Lane (1999) for the failure determination by finite element analyses of slope stability, and discussed in the state-of-the-art paper, geotechnical stability analysis (Sloan 2013). Moreover, it was successfully applied to solve several slope stability problems (e.g., Yu *et al.* 1998, Li *et al.* 2009, 2010, Sloan 2013). Thus, this technique should be valid for this study to solve stability of soil block on a low-interface friction plane, which is one of the slope stability problems. Therefore, it is expected that comparable behaviors at the limit state between physical models and the finite element method with the gravity loading method should be observed.

Table 5 Summary of numerical conditions and the corresponding root-mean-square errors

(a) Slip tests without any shear pins

No:	α (deg.)	W(cm)	L(cm)	T(cm)	L_0 (cm)	Unit weight of silica sand, γ (kN/m ³)	Failure unit weight, γ_f (kN/m ³)
1	39	25	20	1	0	13.68	19.04
2	32.5	25	20	2	0	13.68	15.30
3	30	25	20	3	0	13.68	13.30
4	29	25	20	4	0	13.68	11.42
5	27	25	20	5	0	13.68	12.82
NRMSE = 0.20							

(g) Slip tests with a row of two shear pins with a variation in shear pin location, $T = 1$ cm

No:	α (deg.)	W(cm)	L(cm)	T(cm)	L_0 (cm)	Unit weight of silica sand, γ (kN/m ³)	Failure unit weight, γ_f (kN/m ³)
31	58	20	25	1	1.5	13.68	13.34
32	61	20	25	1	3	13.68	12.41
33	58	20	25	1	4	13.68	13.39
34	67	20	25	1	5	13.68	10.97
35	68	20	25	1	7.5	13.68	11.10
36	69	20	25	1	10	13.68	10.65
37	67	20	25	1	12.5	13.68	10.72
NRMSE = 0.16							

Table 5 Continued

(b) Slip tests with one shear pin at the center

No:	α (deg.)	W(cm)	L(cm)	T(cm)	L_0 (cm)	Unit weight of silica sand, γ (kN/m ³)	Failure unit weight, γ_f (kN/m ³)
6	56	25	20	1	10	13.68	12.16
7	44	25	20	2	10	13.68	11.16
8	41	25	20	3	10	13.68	10.12
9	39	25	20	4	10	13.68	9.61
10	37.5	25	20	5	10	13.68	9.47
NRMSE = 0.24							

(h) Slip tests with a row of two shear pins with a variation in shear pin location, $T = 3$ cm

No:	α (deg.)	W(cm)	L(cm)	T(cm)	L_0 (cm)	Unit weight of silica sand, γ (kN/m ³)	Failure unit weight, γ_f (kN/m ³)
38	54	20	25	3	1.5	13.68	10.80
39	53.5	20	25	3	3	13.68	10.79
40	54	20	25	3	4	13.68	10.88
41	56	20	25	3	5	13.68	10.40
42	57	20	25	3	7.5	13.68	8.52
43	56	20	25	3	10	13.68	7.88
44	57	20	25	3	12.5	13.68	6.99
NRMSE = 0.33							

(c) Slip tests with a row of two shear pins on the horizontal centerline

No:	α (deg.)	W(cm)	L(cm)	T(cm)	L_0 (cm)	Unit weight of silica sand, γ (kN/m ³)	Failure unit weight, γ_f (kN/m ³)
11	59	25	20	1	10	13.68	12.29
12	46	25	20	2	10	13.68	11.56
13	46	25	20	3	10	13.68	9.23
14	44	25	20	4	10	13.68	8.69
15	42	25	20	5	10	13.68	8.81
NRMSE = 0.28							

(i) Slip tests with a row of two shear pins with a variation in shear pin location, $T = 5$ cm

No:	α (deg.)	W(cm)	L(cm)	T(cm)	L_0 (cm)	Unit weight of silica sand, γ (kN/m ³)	Failure unit weight, γ_f (kN/m ³)
45	46	20	25	5	1.5	13.68	14.81
46	48	20	25	5	3	13.68	12.66
47	52	20	25	5	4	13.68	10.40
48	47	20	25	5	5	13.68	11.75
49	50	20	25	5	7.5	13.68	8.94
50	50.5	20	25	5	10	13.68	7.68
51	48	20	25	5	12.5	13.68	7.13
NRMSE = 0.30							

(d) Slip tests with a row of two shear pins on the horizontal centerline, $T = 1$ cm

No:	α (deg.)	W(cm)	L(cm)	T(cm)	L_0 (cm)	Unit weight of silica sand, γ (kN/m ³)	Failure unit weight, γ_f (kN/m ³)
16	89	15	20	1	10	13.68	9.07
17	75	20	20	1	10	13.68	9.83
18	61	25	20	1	10	13.68	11.91
19	58	30	20	1	10	13.68	12.02
20	53	35	20	1	10	13.68	13.10
NRMSE = 0.21							

(j) Slip tests with a column of two shear pins on the vertical centerline, $T = 1$ cm

No:	α (deg.)	W(cm)	L(cm)	T(cm)	L_0 (cm)	Unit weight of silica sand, γ (kN/m ³)	Failure unit weight, γ_f (kN/m ³)
52	49	15	20	1	7.5	13.68	19.10
53	45	20	20	1	7.5	13.68	20.50
54	40.5	25	20	1	7.5	13.68	23.55
55	39	30	20	1	7.5	13.68	24.35
56	38.5	35	20	1	7.5	13.68	24.33
NRMSE = 0.65							

(e) Slip tests with a row of two shear pins on the horizontal centerline, $T = 3$ cm

No:	α (deg.)	W(cm)	L(cm)	T(cm)	L_0 (cm)	Unit weight of silica sand, γ (kN/m ³)	Failure unit weight, γ_f (kN/m ³)
21	49	15	20	3	10	13.68	10.3
22	45	20	20	3	10	13.68	11.2
23	40	25	20	3	10	13.68	12.0
24	37.5	30	20	3	10	13.68	12.9
25	37	35	20	3	10	13.68	12.3
NRMSE = 0.16							

(k) Slip tests with a column of two shear pins on the vertical centerline, $T = 3$ cm

No:	α (deg.)	W(cm)	L(cm)	T(cm)	L_0 (cm)	Unit weight of silica sand, γ (kN/m ³)	Failure unit weight, γ_f (kN/m ³)
57	47.5	15	20	3	7.5	13.68	11.67
58	41	20	20	3	7.5	13.68	13.17
59	38	25	20	3	7.5	13.68	13.63
60	34	30	20	3	7.5	13.68	13.73
61	33	35	20	3	7.5	13.68	16.50
NRMSE = 0.11							

(f) Slip tests with a row of two shear pins on the horizontal centerline, $T = 5$ cm

No:	α (deg.)	W(cm)	L(cm)	T(cm)	L_0 (cm)	Unit weight of silica sand, γ (kN/m ³)	Failure unit weight, γ_f (kN/m ³)
26	48	15	20	5	10	13.68	8.88
27	42	20	20	5	10	13.68	10.48
28	42	25	20	5	10	13.68	8.68
29	36	30	20	5	10	13.68	11.02
30	35	35	20	5	10	13.68	10.84
NRMSE = 0.28							

(l) Slip tests with a column of two shear pins on the vertical centerline, $T = 5$ cm

No:	α (deg.)	W(cm)	L(cm)	T(cm)	L_0 (cm)	Unit weight of silica sand, γ (kN/m ³)	Failure unit weight, γ_f (kN/m ³)
62	45	15	20	5	7.5	13.68	10.70
63	40	20	20	5	7.5	13.68	11.45
64	37	25	20	5	7.5	13.68	11.42
65	34	30	20	5	7.5	13.68	12.53
66	33	35	20	5	7.5	13.68	12.38
NRMSE = 0.15							

Finite element analyses with the gravity loading method were performed according to geometrical conditions of physical models, as shown in Table 5. Each finite element model

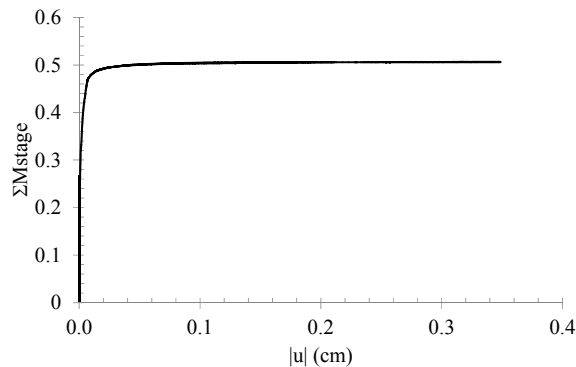


Fig. 7 Demonstration of failure analysis using the gravity loading method in Plaxis 3D

employed a different slope angle that is equal to a failure slope angle (α_f) measured from each test, as listed in the second column in Table 5. Thus, the accuracy of finite element simulation was assessed by the difference between a computed failure unit weight and the actual soil unit weight.

Fig. 7 shows an example of the solution to the gravity loading analysis by plotting the relationship of the ΣM_{stage} value at each step versus the displacement of a selected point. The curve tends to be flat and reaches a state of convergence at the final step. This result confirms that the limit state of this case is successfully solved by a finite element simulation.

Typically, the computational time of a slip test with shear pins is 4-8 hours for each simulation. The finite element simulations were performed on a Samsung Notebook, whose specifications are Intel (R) Core (TM) i7-3630 QM CPU@2.4 Ghz, 8 GB RAM and Windows7 Enterprise.

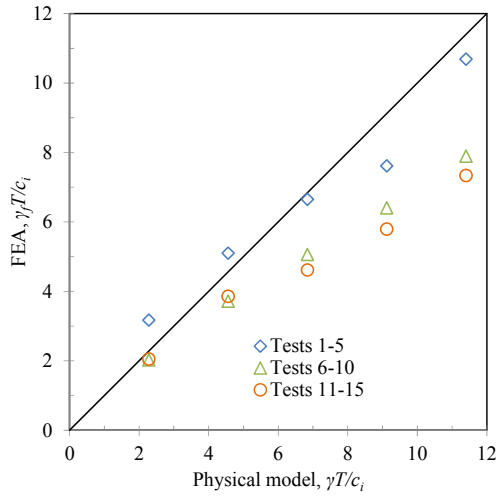
4. Results and discussions of 3D finite element analysis

4.1 Slip tests without any shear pins and with one shear pin at the center

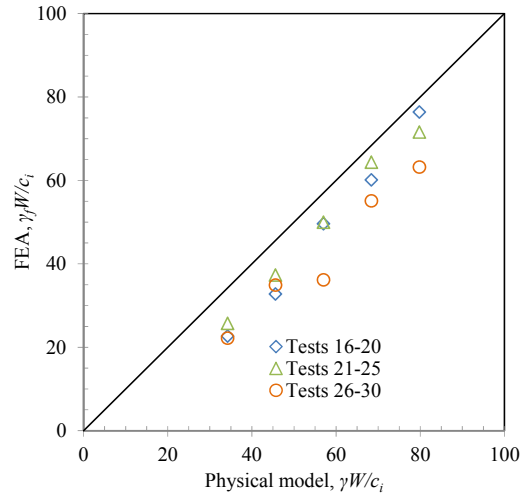
The first results of the three-dimensional finite element analyses correspond to the cases of the slip tests on two models, one without any shear pins and the other with one shear pin at the center. Figs. 2(a) and 6(a) show the physical and the numerical models without any shear pins, respectively. Figs. 2(b) and 6(b) show the numerical and the physical models with one shear pin at the center, respectively. The same dimensions are used in both cases, with and without a shear pin, following those of the physical models. The soil block has a length of $L = 20$ cm and a width of $W = 25$ cm; it rests on a low-interface friction plane with slope angle α . The thickness of the soil block, T , varies from 1 to 5 cm.

Table 5 summarizes the numerical results for all the geometries of the slip tests by which the accuracy of the prediction is evaluated through the normalized root-mean-square error (NRMSE) between the actual unit weight ($\gamma = 13.68$ kN/m³) of the soil block and the predicted failure soil unit weight (γ_f) at failure. NRMSE is defined as the square root of the mean of the squares of the deviations between predicted failure and actual soil unit weights, which is normalized by the actual soil unit weight, as shown in Eq. (2).

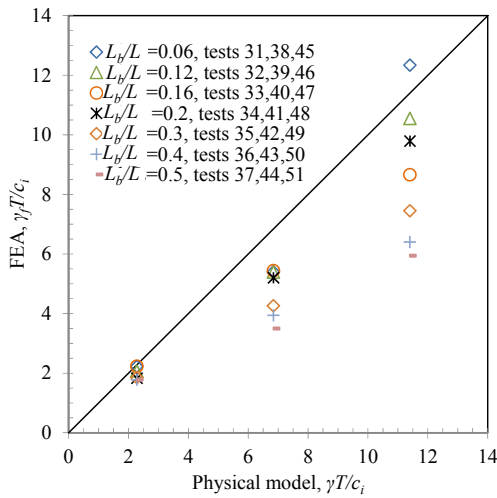
$$NRMSE = \frac{1}{\gamma} \sqrt{\frac{\sum_{i=1}^n (\gamma_{f,i} - \gamma)^2}{n}} \quad (2)$$



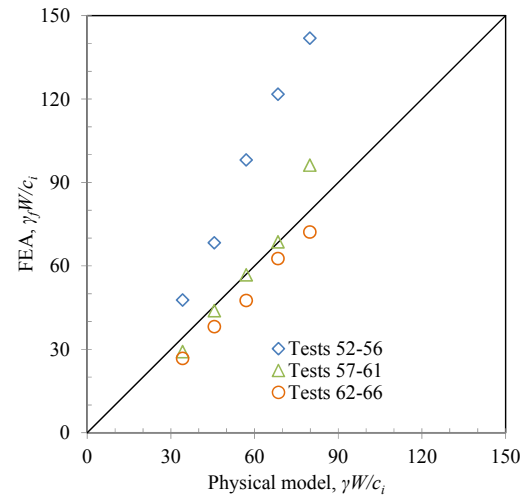
(a) Slip tests without any shear pins, with one pin at the center and with two shear pins on the horizontal centerline



(b) Slip tests with a row of two shear pins on the horizontal centerline, $T = 1, 3$ and 5 cm



(c) Slip tests with a row of two shear pins with a variation in shear pin location, $T = 1, 3$ and 5 cm



(d) Slip tests with a column of two shear pins on the vertical centerline, $T = 1, 3$ and 5 cm

Fig. 8 Comparisons of stability number between physical and numerical models

where $\gamma_{f,i}$ = predicted failure soil unit weight of i^{th} model obtained from finite element analysis
 n = total number of models in each set of simulation
 γ = actual soil unit weight = 13.68 kN/m^3

Fig. 8 shows comparisons of the stability number between the numerical and the physical models for all cases. In most cases, the stability number of the physical models is greater than that of the numerical models, except for cases no. 52-56 (Fig. 8(d)), where the stability number of the

numerical models is significantly larger than that of the physical models.

In order to confirm that the condition of the fully rough shear pin is more suitable than the condition of the fully smooth shear pin when modelling screw bolts, some of the corresponding NRMSEs of the two conditions are compared. The NRMSEs for tests no. 6-10, no. 11-15 and no. 16-20, under the fully smooth shear pin condition (smooth results not shown Table 5), are 0.31, 0.33 and 0.26, respectively, while those under the fully rough shear pin condition are 0.24, 0.28 and 0.21, respectively. As NRMSEs in the latter case are lower, the fully rough shear pin condition was therefore chosen for use in all the numerical analyses.

Fig. 9 shows the stability number, $\gamma_f T/c_i$, as a function of the failure slope angle, α_f , for the numerical analyses with and without shear pins by the finite element analysis. The results of the slip tests with the physical models, with and without a shear pin, are also plotted in this figure. The trends in the stability number of the finite element analysis are similar to those of the physical models for both cases. The failure slope angle has a nonlinear inverse relationship to the thickness of the soil block. The smaller thickness of the soil block corresponds to the larger failure slope angle. The NRMSEs between the physical and the numerical models of the slip tests with one shear pin at the center and without any shear pins are around 0.24 and 0.20, respectively.

Fig. 10 shows the numerical results of the slip test without any shear pins for test no. 3. As shown in Figs. 10(a)-(b), the incremental displacement is uniform for all parts of the soil block, indicating the translation failure mechanism. The results of the relative shear stress ratio, which is a ratio of the shear resistance in respect to the current shear stress in Fig. 10(c), reveal that no failure happens inside the soil block, where the applied shear stress is less than the shear strength of the soil block. On the other hand, there is failure on the interface plane, where the relative shear stress ratio is unity, as shown in Fig. 10(d). Thus, the failure mechanism of the soil block without any shear pins is only due to shear sliding on the low-interface friction plane.

Fig. 11 shows the results of the slip test with one shear pin at the center for test no. 8. The relatively small incremental soil displacement above the shear pin displayed in Fig. 11(b) indicates that some parts of soil block are resisted by the shear pin. On the other hand, large incremental soil displacement occurs below the shear pin. The failure of the soil occurs around the shear pin and expands vertically and laterally to the top edge, where the relative shear stress ratio of those zones

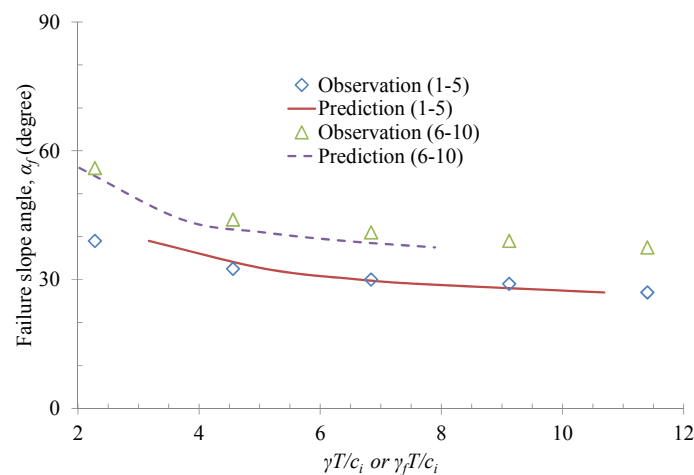
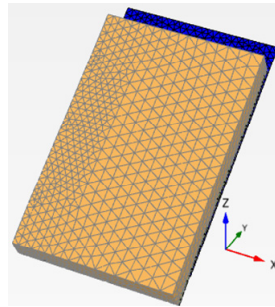
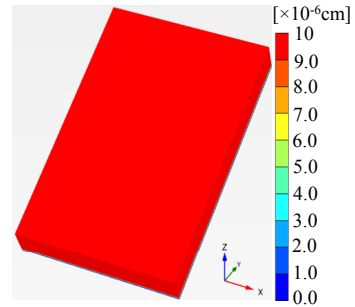


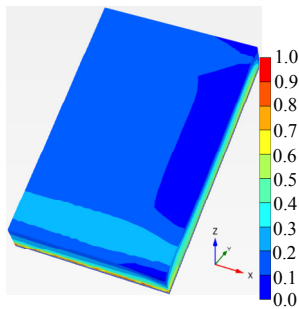
Fig. 9 Variations in failure slope angle versus stability number



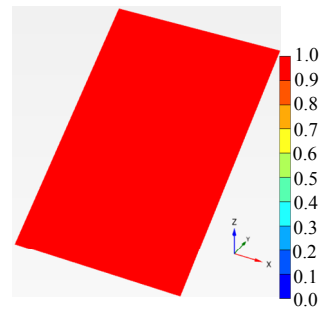
(a) Deformed mesh, $|u|$



(b) Incremental displacement, $|\Delta u|$

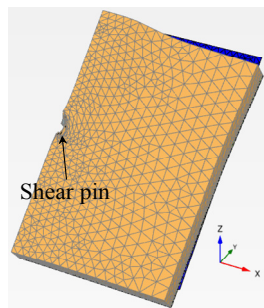


(c) Relative shear stress ratio of top soil block, τ_{rel}

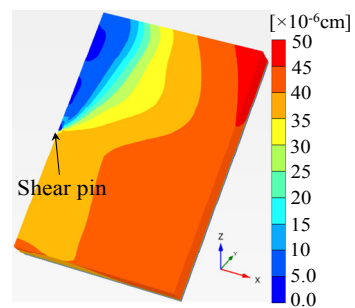


(d) Relative shear stress ratio of interface plane, τ_{rel}

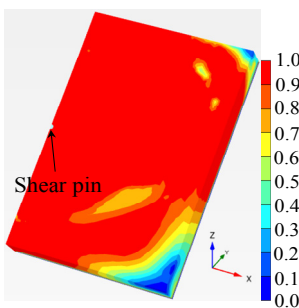
Fig. 10 Results of finite element analysis of slip test without any shear pins for test no. 3



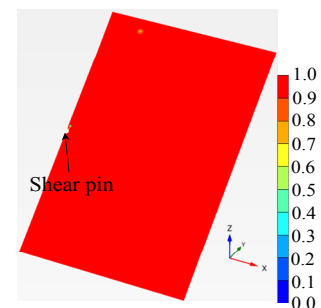
(a) Deformed mesh, $|u|$



(b) Incremental displacement, $|\Delta u|$



(c) Relative shear stress ratio of top soil block, τ_{rel}



(d) Relative shear stress ratio of interface plane, τ_{rel}

Fig. 11 Results of finite element analysis of slip test with one shear pin at the center for test no. 8

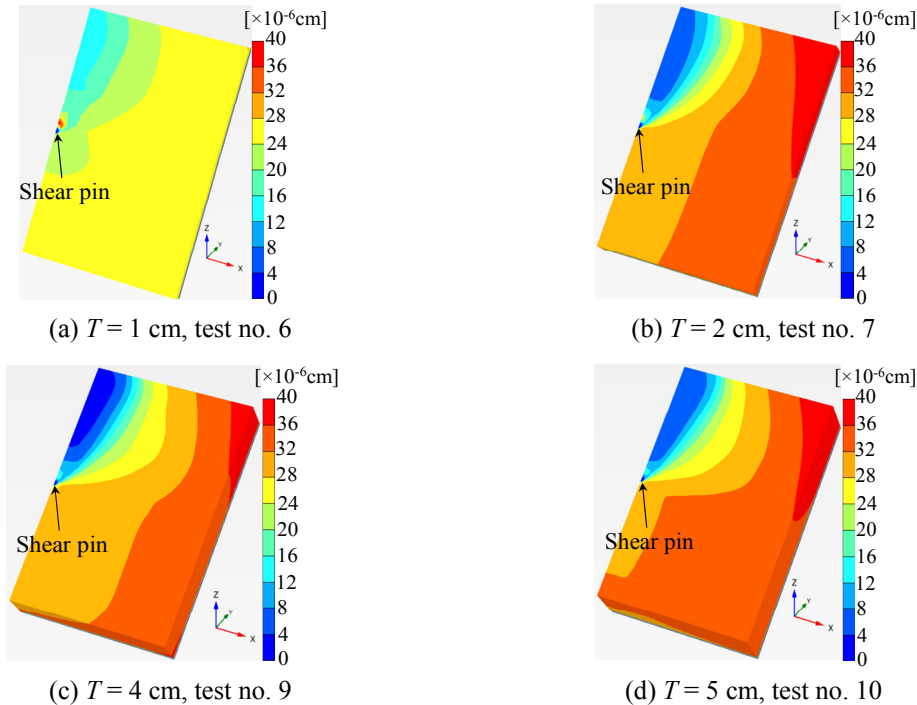


Fig. 12 Comparisons of incremental displacement of slip test with one shear pin at the center with a variation in soil thickness

reaches unity, as shown in Fig. 11(c). The remaining soil parts, including the lower and the surrounding parts of the shear pin, where the relative shear stress ratio is less than unity, do not fail. The results of the low-interface friction plane in Fig. 11(d) indicate that the interface shearing resistance is mobilized on the interface plane. Thus, the results show that the failure of this model is attributed to the shear sliding of the soil block on the low-interface friction plane together with the local failure of the soil block above the shear pin. Fig. 12 compares the incremental displacement of the slip test with one shear pin at the center with the variation in soil thickness. The patterns of incremental displacement are comparable for different values of soil thickness. Smaller incremental soil displacement appears above the shear pin, while larger incremental soil displacement occurs in the remaining parts.

4.2 Slip test with a row of two shear pins on the horizontal centerline

The next results for the three-dimensional finite element analyses correspond to the case of the slip test on the model with a row of two shear pins on the horizontal centerline, as shown in Fig. 6(c). The physical model for this case is shown in Fig. 2(c). Fig. 13 shows all the comparisons of the stability number between the physical models and the finite element analyses for the three cases, namely, the slip test without any shear pins, the slip test with one shear pin at the center and the slip test with a row of two shear pins on the horizontal centerline. The trend of the computed stability number of the slip test with a row of two shear pins on the horizontal centerline is qualitatively comparable to that of the physical model. A larger thickness of the soil block is

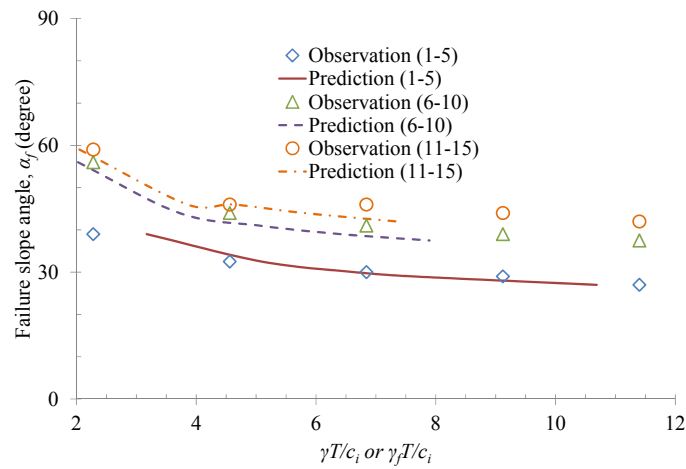


Fig. 13 Comparisons of failure slope angle versus stability number between the case without any shear pins, the case with one shear pin at the center and the case with two shear pins on the horizontal centerline

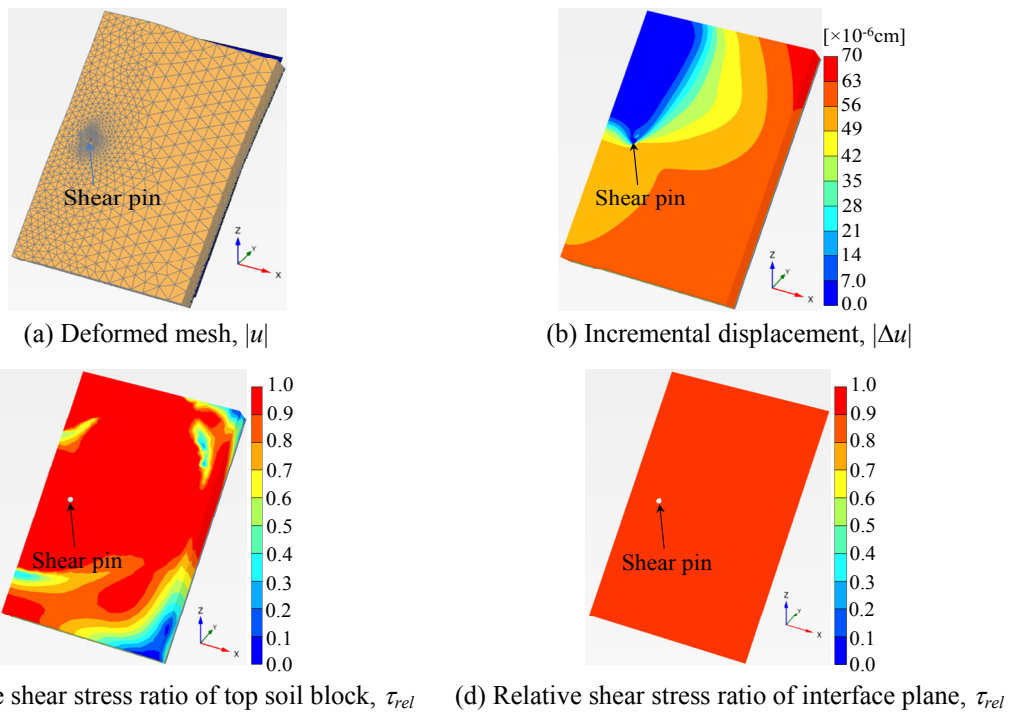


Fig. 14 Results of the finite element analysis of the slip test with a row of two shear pins on the horizontal centerline for test no. 13

related to a smaller failure slope angle. The NRMSE between the physical and the numerical models of the slip test with a row of two shear pins on the horizontal centerline is 0.28. The curve in the case of two shear pins is located on the top of the chart, followed by that of one shear pin and then the case without any shear pins.

Fig. 15 shows comparisons of the incremental displacement of the slip test with a row of two shear pins on the horizontal centerline with a variation in soil thickness. The patterns of incremental displacement are comparable for all cases, where very small incremental displacement of the soil is observed above the shear pins. Therefore, the finite element analyses indicate that the failure of the soil block with a row of two shear pins is due to shear sliding on the low-interface friction plane together with the occurrence of punching shear failure on the soil block in front of the shear pins. On the other hand, detachment failure was observed in the physical model, where an open crack started to develop along the row of shear pins and extended horizontally to the edge of the soil block. As a result, the block below the row of shear pins slipped down along the slope, but the top part above the shear pins was still stable. This actual failure mechanism cannot be realized in those finite element results.

Fig. 16 shows the parametric studies of the finite element analysis with a row of two shear pins on the horizontal centerline with the variation in soil width, where $L = 20$ cm, $T = 1, 3$ and 5 cm and $W = 15-35$ cm. In this figure, the term $\gamma_f W/c_i$ is used instead of $\gamma_f T/c_i$, since both the slope angle and the soil width are varied, but the soil thickness and the length are kept constant. The results of the stability number of the soil block with a row of two shear pins depend on the width of the soil block in addition to its thickness. Note that for the case of the slip test without any shear pins, the stability number was independent of the soil block width (after Khosravi 2012). The NRMSEs between the physical and the numerical models of the slip test with a row of two shear pins on the horizontal centerline, with the variation in soil width, are 0.21, 0.16 and 0.28 for $T = 1, 3$ and 5 cm, respectively.

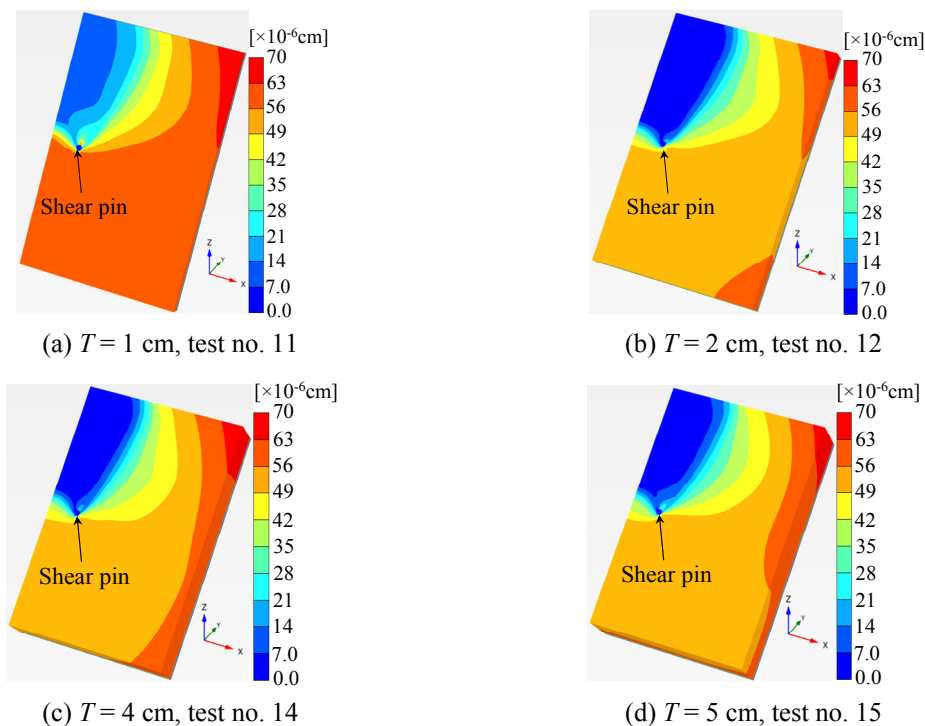


Fig. 15 Comparisons of incremental displacement of the slip test with a row of two shear pins on the horizontal centerline with a variation in soil thickness

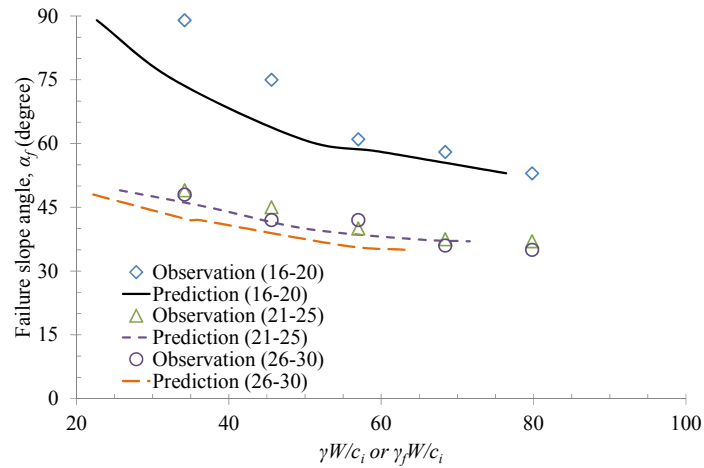


Fig. 16 Failure slope angle versus stability number of slip test with a row of two shear pins on the horizontal centerline with a variation in soil width

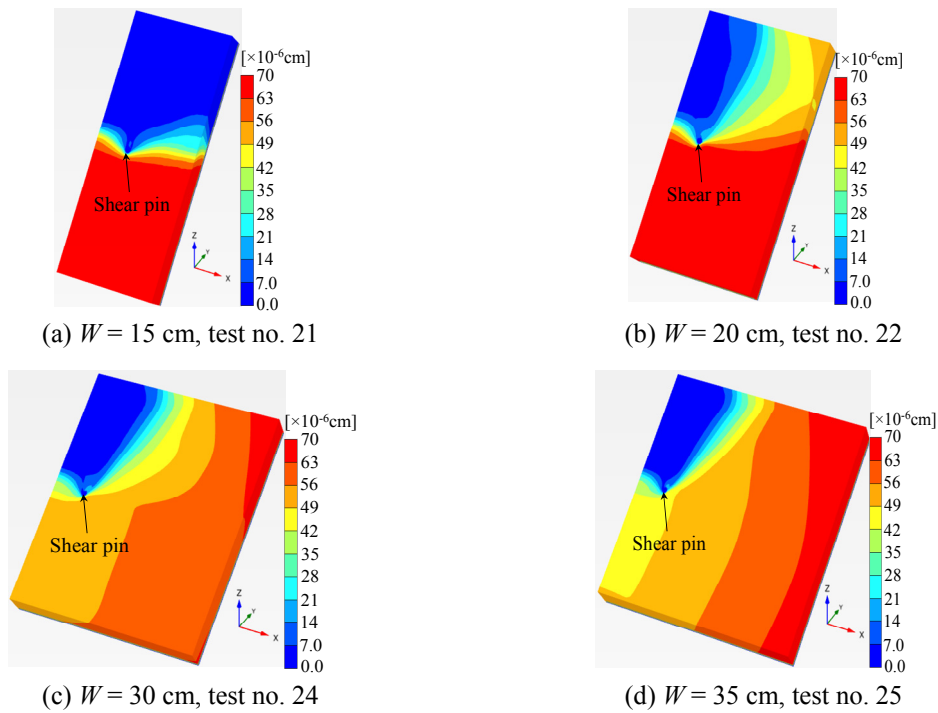


Fig. 17 Comparisons of incremental displacement of slip test with a row of two shear pins on the horizontal centerline with a variation in soil width for the case $T = 3$ cm

Figs. 17-18 show comparisons of the incremental displacement of the slip tests with a row of two shear pins on the horizontal centerline with a variation in soil width for the cases $T = 3$ cm and $T = 5$ cm, respectively. A very small difference in incremental displacement is observed between these two cases. For a narrow soil width, the size of the stable part covers the full width of the soil

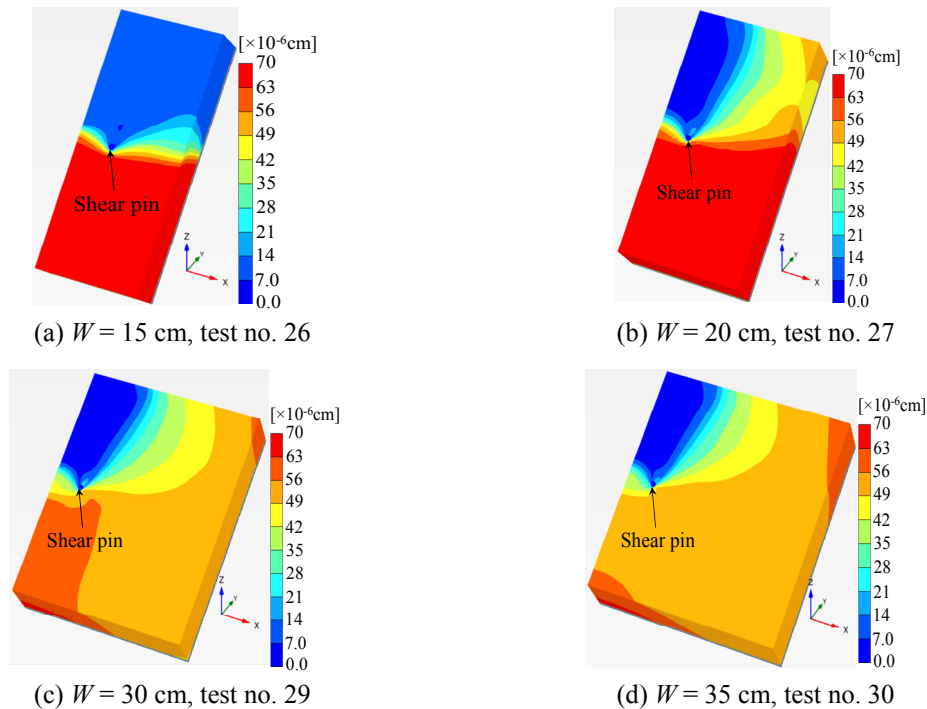


Fig. 18 Comparisons of incremental displacement of slip test with a row of two shear pins on the horizontal centerline with a variation in soil width for the case $T = 5$ cm

block and extends to its sides. As the width of the soil block increases, the size of the stable part decreases and covers only the central zone in front of the shear pins. Thus, the size of the stable part above the shear pins depends on the width of the soil block.

4.3 Slip test with a row of two shear pins with variation in their locations

Parametric studies are also carried out to investigate the influence of the location of a row of two shear pins on the increase in the stability of the slip test, where their locations (L_b) are the distances which are measured from the bottom edge of the soil block and varied from 1.5 cm to 12.5 cm, as shown in Fig. 6(d). The physical model of this simulation is shown in Fig. 2(d). In addition, three values of soil thickness are used, i.e., $T = 1, 3$ and 5 cm, where $W = 20$ cm and $L = 25$ cm. Fig. 19 compares the results of the failure slope angle versus the stability number between the numerical models and the physical models for those parametric studies of the shear pin locations. There is a qualitatively reasonable agreement in stability number between the numerical models and the physical models when $L_b/L \leq 0.2$. However, when $L_b/L > 0.2$, a larger difference in stability number between the numerical models and the physical models can be observed. The numerical results show that the location of the row of two shear pins affects the stability of the soil block, but that only a very small difference in the results can be observed from the physical models. Based on the numerical results, a row of two shear pins on the horizontal centerline generally gives the lowest stabilization. The highest stabilization depends on the thickness of the soil block. For a large thickness of the soil block, the best stabilization corresponds to the shear pin location

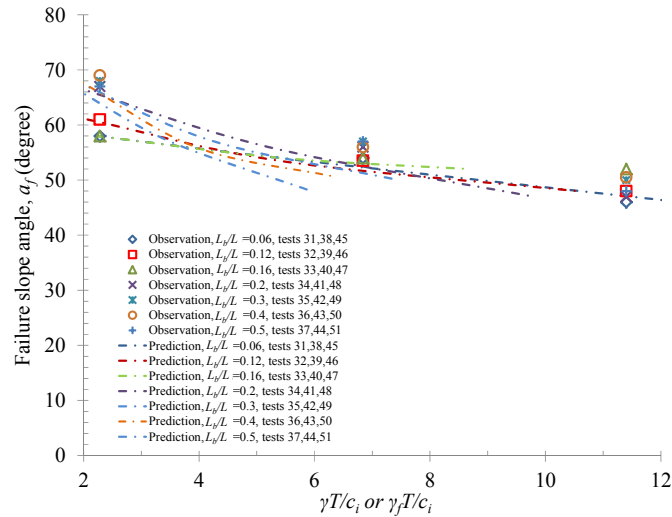


Fig. 19 Variations in failure slope angle versus stability number of slip tests with a row of two shear pins and in the shear pin location

near the toe of the slope ($L_b/L = 0.06$). On the other hand, the location of $L_b/L = 0.2$ gives the highest stabilization of a small thickness of the soil block. These observations correspond to the results reported by Ausilio *et al.* (2001), where the most effective pile location is within the region from the middle to the toe of the slope.

Figs. 20-22 show comparisons of the incremental displacement of the slip test with a row of two shear pins and variations in shear pin location for cases $T = 1, 3$ and 5 cm, respectively. In general, the patterns of the incremental displacement depend on the locations of the pins and the soil thickness. The influence of the shear pin location gives rise to a clear separation between the very small displacement of the soil block above the shear pins and the large displacement of the soil block below the shear pins and the remaining parts. Different patterns of incremental

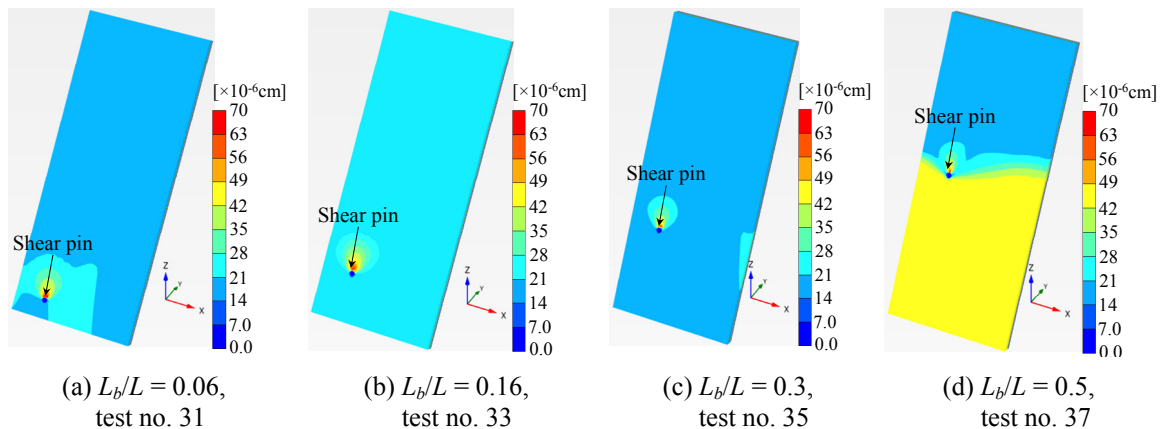


Fig. 20 Comparisons of incremental displacement of slip test with a row of two shear pins with a variation in shear pin location for the case $T = 1$ cm

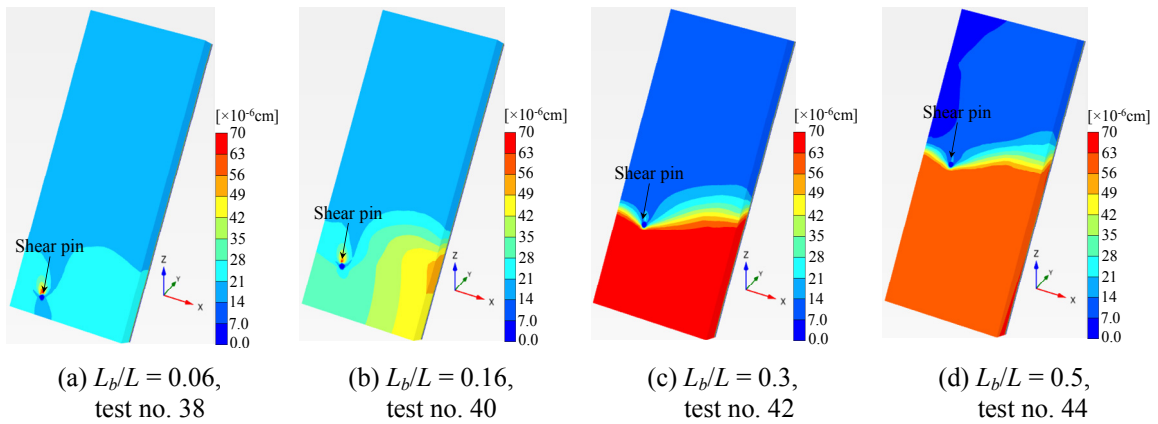


Fig. 21 Comparisons of incremental displacement of slip test with a row of two shear pins with a variation in shear pin location for the case $T = 3$ cm

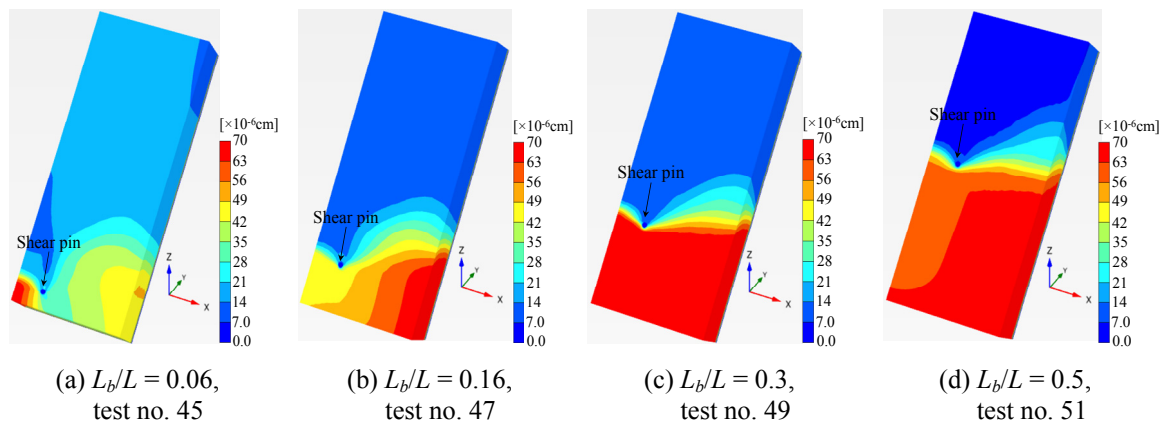


Fig. 22 Comparisons of incremental displacement of slip test with a row of two shear pins with a variation in shear pin location for the case $T = 5$ cm

displacement can be observed for the case with the same value for L_b/L , but with different values for soil thickness. For all values of soil thickness, the zone of the stable part can be observed when $L_b/L \geq 0.3$, indicating that the stable part above the shear pins depends on the thickness of the soil block and the locations of the shear pins. The NRMSEs between the physical and the numerical models of the slip tests in these cases are 0.16, 0.33 and 0.30 for $T = 1, 3$ and 5 cm, respectively.

4.4 Slip test with a column of two shear pins on the vertical centerline

The last of the three-dimensional finite element analyses corresponds to the case of a column of two shear pins installed on the vertical centerline, as shown in Fig. 6(e). Fig. 2(e) shows the physical model of this problem. Three thicknesses of the soil block are set up as 1, 3 and 5 cm, and its width is varied from 15 to 35 cm, where $L = 20$ cm.

Fig. 23 shows the results of the failure slope angle versus the stability number, $\gamma W/c_i$, of the

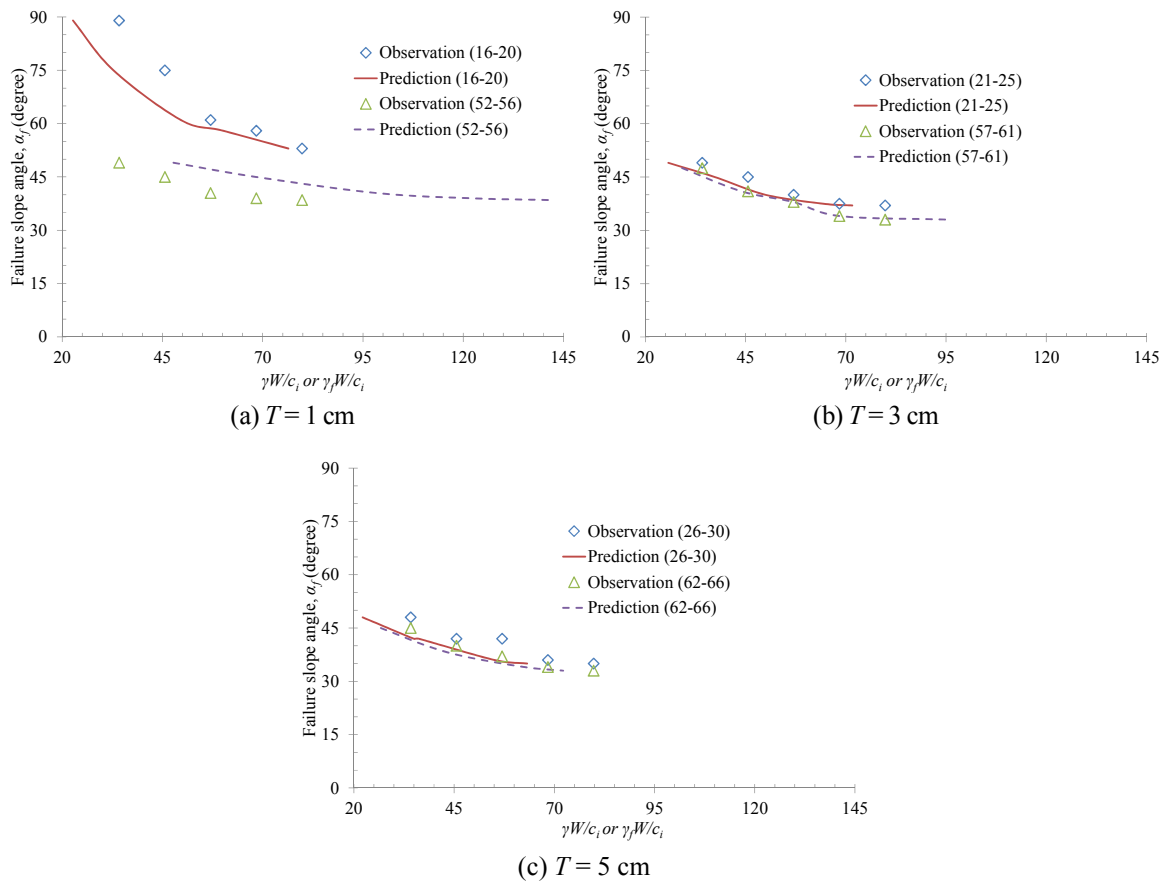


Fig. 23 Comparisons of failure slope angle versus stability number for different arrangements of two shear pins

slip test for different shear pin arrangements. According to Figs. 23(b)-(c), the results of the numerical model with a row of two shear pins on the horizontal centerline give higher slope stabilization than those of a column of two shear pins.

It should be noted that for the case of $T = 1$ cm, the failure slope angles of the physical models with a row of two shear pins (Fig. 23(a)) are significantly higher than those of a column of two shear pins. However, for the cases of $T = 3$ cm and 5 cm (Figs. 23(b)-(c)), there are no significant differences between the results of a row of two shear pins and of a column of two shear pins for either the experimental or the numerical results.

Fig. 24 shows the incremental displacement of the slip test with a column of two shear pins on the vertical centerline for the case $T = 3$ cm. The failure mechanism of a column of two shear pins observed from the incremental soil displacement depends on the width of the soil block. For the large width of a slope, the zone of very small incremental displacement starts from the lower shear pin and encloses the upper shear pin in a narrow region. The size of this zone expands more laterally than the zone with one shear pin, resulting in higher stability. The NRMSEs between the physical and the numerical models of slip tests in these cases are 0.65, 0.11 and 0.15 for $T = 1, 3$ and 5 cm, respectively.

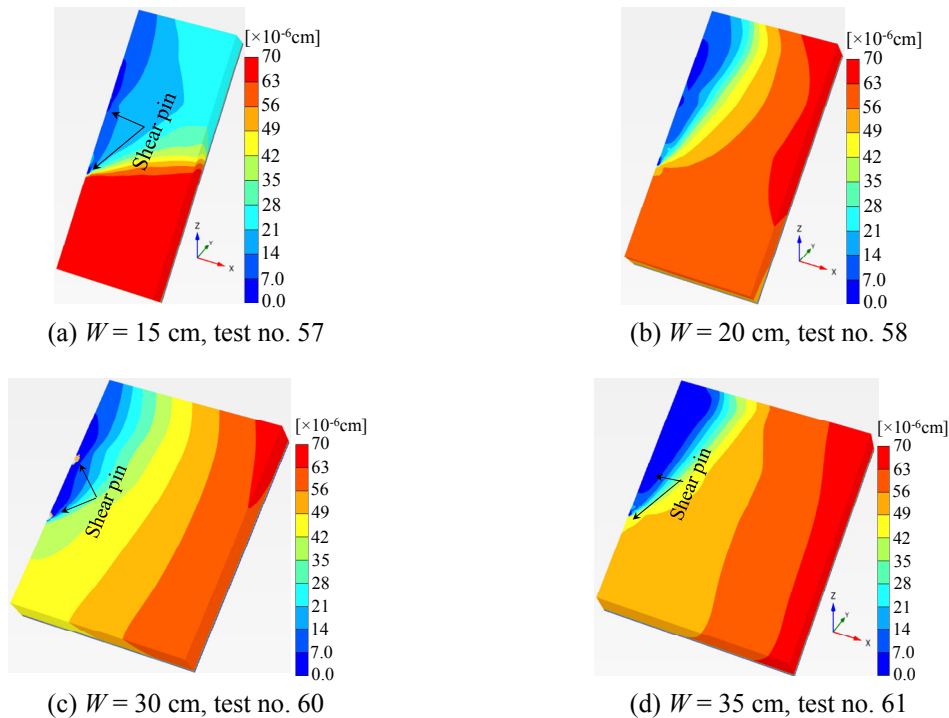


Fig. 24 Comparisons of incremental displacement of slip test with a column of two shear pins on the vertical centerline for the case $T = 3$ cm

5. Conclusions

In this paper, three-dimensional finite element analyses were employed to investigate the performance of shear pin arrangements on the stability of a soil block resting on a low-interface friction plane. Four series of finite element analyses with different arrangements of shear pins were performed in order to understand the influence of the shear pin arrangement on slope stabilization. In the numerical models, the soil block and the interface elements were modeled by Mohr-Coulomb material. The interface elements at the bedding plane were used to characterize shear sliding on the interface plane. The interface elements around the shear pins were modeled as a fully rough surface. The bedding plane and the shear pins were modeled by linear elastic material. The gravity loading method was used to simulate the failure of this problem in the three-dimensional finite element analyses. The important conclusions can be summarized as follows:

- For all cases, the results of the stability number obtained from each finite element analysis were qualitatively comparable to those of the physical models. Thus, the modeling technique with the gravity loading method employed in this study is capable of reasonably simulating the failure of a soil block reinforced by shear pins and resting on a low-interface friction plane.
- By employing physical models and limit equilibrium method, Khosravi (2012) found that the stability number of soil block without shear pin was dependent on only the thickness of soil block. It is expected that the lower stability number of the problem with shear pins is

related to a thicker thickness or a wider width of the soil block. In this study, both experimental and numerical results confirmed that the stability number of soil block with shear pins had a reversely nonlinear relationship to the thickness and the width of the soil block. In addition, the stability number curve of soil blocks without shear pin represented the lowest limit of all curves with shear pins because of a strengthening effect of soil block by shear pin.

- For all shear pin arrangements, shear sliding occurred at a low interface friction of the bedding plane. In addition, there was a distinct separation between the zone of very small incremental displacement, happening above the shear pins, and the zone of very large incremental displacement, happening below the shear pins and the remaining parts. The failure mechanism of the soil block with one shear pin consisted of a local failure above the shear pin. A stable zone developed for the case with a row of two shear pins on the horizontal centerline. For a smaller width of soil block, the size of failure mechanism was highly influenced by its boundary and largely dominated by an effect of high value of dilation angle. However, it was expected that when increasing the width of soil block, these two effects became less influenced and disappeared. Hence, the size of failure mechanism did not significantly change with an increase of the width of soil block.
- According to the numerical results, the optimal location depended on the thickness of the soil block. For a thick slope, the best location was found to be near the toe of the slope. In contrast, for a thin slope, the best location was found to be between the toe and the middle of the slope.
- For different arrangements of two shear pins, the one which was found to give the highest stabilization is the row of shear pins on the horizontal centerline, followed by the column of shear pins on the vertical centerline.

The results of this study are useful for the theoretical development of slope reinforcement for civil and surface mining projects.

Acknowledgments

This research was funded by the Electricity Generating Authority of Thailand (EGAT) and the ASEAN University Network/Southeast Asia Engineering Education Department Network (AUN/SEED-Net) Ph.D. Sandwich Program under the Japanese International Cooperation Agency (JICA). The first author would like to express his gratitude to AUN/SEED-Net for the financial support of the research fellowship program in Japan.

References

- Ausilio, E., Conte, E. and Dente, G. (2001), "Stability analysis of slopes reinforced with piles", *Comput. Geotech.*, **28**(8), 591-611.
- Brinkgreve, R. (2012), *Plaxis 3D 2012*, Plaxis Bv, Netherlands.
- Brinkgreve, R., Swolfs, W., Engin, E., Waterman, D., Chesaru, A., Bonnier P. and Galavi V. (2013), *PLAXIS 3D Reference Manual*, Plaxis Bv, Netherlands.
- Chen, W.F. (1975), *Limit Analysis and Soil Plasticity*, Elsevier Amsterdam, Netherlands.
- Fatahi, B., Basack, S., Ryan, P., Zhou, W.-H. and Khabbaz, H. (2014), "Performance of laterally loaded piles considering soil and interface parameters", *Geomech. Eng., Int. J.*, **7**(5), 495-524.

- Galli, A. and di Prisco, C. (2012), "Displacement-based design procedure for slope-stabilizing piles", *Can. Geotech. J.*, **50**(1), 41-53.
- Griffiths, D. and Lane, P. (1999), "Slope stability analysis by finite elements", *Geotechnique*, **49**(3), 387-403.
- Haigh, S.K. and Gopal Madabhushi, S. (2011), "Centrifuge modelling of pile-soil interaction in liquefiable slopes", *Geomech. Eng., Int. J.*, **3**(1), 1-16.
- Ho, I.-H. (2014), "Numerical study of slope-stabilizing piles in undrained clayey slopes with a weak thin layer", *Int. J. Geomech.*, 06014025-1-12.
- Ito, T. and Matsui, T. (1975), "Methods to estimate lateral force acting on stabilizing piles", *Soils Found.*, **15**(4), 43-59.
- Ito, T., Matsui, T. and Hong, W.P. (1982), "Extended design method for multi-row stabilizing piles against landslide", *Soils Found.*, **22**(1), 1-13.
- Kanagasabai, S., Smethurst, J. and Powrie, W. (2011), "Three-dimensional numerical modelling of discrete piles used to stabilize landslides", *Can. Geotech. J.*, **48**(9), 1393-1411.
- Keawsawasvong, S. and Ukritchon, B. (2017), "Undrained limiting pressure behind soil gaps in contiguous pile walls", *Comput. Geotech.*, **83**, 152-158.
- Khosravi, M.H. (2012), *Arching Effect in Geomaterials with Applications to Retaining Walls and Undercut Slopes*, Doctor of Philosophy, Tokyo Institute of Technology.
- Khosravi, M.H., Pipatpongsa, T., Takahashi, A. and Takemura, J. (2011), "Arch action over an excavated pit on a stable scarp investigated by physical model tests", *Soils Found.*, **51**(4), 723-735.
- Khosravi, M.H., Tang, L., Pipatpongsa, T., Takemura, J. and Doncommul, P. (2012), "Performance of counterweight balance on stability of undercut slope evaluated by physical modeling", *Int. J. Geotech. Eng.*, **6**(2), 193-205.
- Kourkoulis, R., Gelagoti, F., Anastasopoulos, I. and Gazetas, G. (2011), "Slope stabilizing piles and pile-groups, parametric study and design insights", *J. Geotech. Geoenviron. Eng.*, **137**(7), 663-677.
- Kourkoulis, R., Gelagoti, F., Anastasopoulos, I. and Gazetas, G. (2012), "Hybrid method for analysis and design of slope stabilizing piles", *J. Geotech. Geoenviron. Eng.*, **138**(1), 1-14.
- Li, L. and Liang, R.Y. (2014), "Limit equilibrium based design approach for slope stabilization using multiple rows of drilled shafts", *Comput. Geotech.*, **59**, 67-74.
- Li, A.J., Merifield, R. and Lyamin, A. (2009), "Limit analysis solutions for three dimensional undrained slopes", *Comput. Geotech.*, **36**(8), 1330-1351.
- Li, A.J., Merifield, R. and Lyamin, A. (2010), "Three-dimensional stability charts for slopes based on limit analysis methods", *Can. Geotech. J.*, **47**(12), 1316-1334.
- Li, X., He, S., Luo, Y. and Wu, Y. (2011), "Numerical studies of the position of piles in slope stabilization", *Geomech. Geoeng.*, **6**(3), 209-215.
- Liang, R.Y., Joorabchi, A.E. and Li, L. (2014), "Analysis and design method for slope stabilization using a row of drilled shafts", *J. Geotech. Geoenviron. Eng.*, **140**(5), 04014001.
- Madhav, M.R., Sharma, J. and Sivakumar, V. (2009), "Settlement of and load distribution in a granular piled raft", *Geomech. Eng., Int. J.*, **1**(1), 97-112.
- Nakanishi, K. and Takewaki, I. (2013), "Optimum pile arrangement in piled raft foundation by using simplified settlement analysis and adaptive step-length algorithm", *Geomech. Eng., Int. J.*, **5**(6), 519-540.
- Ouch, R., Ukritchon, B. and Pipatpongsa, T. (2016), "Stability of soil block on low interface friction plane with and without side supports", *Eng. J.*, **20**(2), 123-145.
- Pipatpongsa, T., Khosravi, M. and Takemura, J. (2013), "Physical modeling of arch action in undercut slopes with actual engineering practice to Mae Moh open-pit mine of Thailand", *Proceedings of the 18th International Conference on Soil Mechanics and Geotechnical Engineering (ICSMGE18)*, Paris, France, September.
- Poulos, H.G. (1995), "Design of reinforcing piles to increase slope stability", *Can. Geotech. J.*, **32**(5), 808-818.
- Pradel, D., Garner, J. and Kwok, A.O.L. (2010), "Design of drilled shafts to enhance slope stability", *Geotechnical Special Publication*, **384**(208 GSP), 920-927.

- Qian, Z.Z., Lu, X.L., Yang, W.Z. and Cui, Q. (2014), "Behaviour of micropiles in collapsible loess under tension or compression load", *Geomech. Eng., Int. J.*, **7**(5), 477-493.
- Sloan, S.W. (2013), "Geotechnical stability analysis", *Géotechnique*, **63**(7), 531-572.
- Wei, W.B. and Cheng, Y.M. (2009), "Strength reduction analysis for slope reinforced with one row of piles", *Comput. Geotech.*, **36**(7), 1176-1185.
- Wu, Y., Yamamoto, H. and Yao, Y. (2013), "Numerical study on bearing behavior of pile considering sand particle crushing", *Geomech. Eng., Int. J.*, **5**(3), 241-261.
- Yu, H., Salgado, R., Sloan, S.W. and Kim, J. (1998), "Limit analysis versus limit equilibrium for slope stability", *J. Geotech. Geoenviron. Eng.*, **124**(1), 1-11.
- Zhang, G., Tan, J., Zhang, L. and Xiang, Y. (2015), "Linear regression analysis for factors influencing displacement of high-filled embankment slopes", *Geomech. Eng. Int. J.*, **8**(4), 511-521.
- Zhou, C., Shao W. and Westen, C.J.V. (2014), "Comparing two methods to estimate lateral force acting on stabilizing piles for a landslide in the Three Gorges Reservoir, China", *Eng. Geol.*, **173**, 41-53.